J. Fluid Mech. (1982), *vol.* 121, *pp.* 315–343
Printed in Great Britain

On the development of fluid trapping beneath deformable fluid-cell membranes

By RANDALL WU† AND SHELDON WEINBAUM

Department of Mechanical Engineering, The City College of
The City University of New York, New York, NY 10031

(Received 5 March 1981 and in revised form 28 December 1981)

A quantitative theoretical model is developed to describe the time-dependent draining of an initially uniform-thickness fluid squeeze film between an infinitely flexible membrane-bound fluid cell and a planar rigid surface or between two symmetrically loaded cells subject to impulsive loading. The solution of the coupled nonlinear membrane–fluid-film equations shows that two characteristic times and lengthscales are required to describe the membrane deformation and draining behaviour of the fluid film. The early-time behaviour is strikingly different from that predicted by elastohydrodynamic squeeze-film theory (Christensen 1962), where the local elastic deformation of the boundary is not controlled by membrane tension but is proportional to the local film pressure. While fluid trapping occurs in both cases, a bi-directional flow is set up during the early-time period in the membrane squeeze film owing to the establishment of an off-axis pressure maximum near the edge of the near-contact area. Fluid is driven radially inward, causing upwelling of the membrane in the central region, and driven radially outward near the edge of the contact area, causing this region to form a narrow fluid gap. After the narrow-edge region has formed, the off-axis pressure maximum gradually disappears and is replaced by a pressure plateau in the interior and a radial outflow at all locations that is similar to the elastohydrodynamic squeeze film. The present problem is closely related to the fluid films studied by Hartland (1967, 1968, 1969), Jones & Wilson (1978) and others when a small spherical particle or fluid droplet rises or settles under gravity towards a uniform-tension fluid–fluid interface. These studies have theoretically and experimentally examined the long-time drainage of the film after the narrow edge region has formed and the fluid-trapping phenomenon is established. The solutions to the initial-value problem described herein show how this asymptotic quasi-steady drainage state is reached.

A simple experiment has been constructed to confirm qualitatively the theoretically predicted short-time behaviour. Experimental photographs graphically illustrate the gradual thickening of the lubricating layer near the origin and the formation and draining of the edge region as predicted by the membrane squeeze-film theory.

1. Introduction

The time-dependent draining of a fluid film between a rigid planar surface and a highly flexible membrane-bound fluid cell or between two membrane-bound fluid cells is a problem of fundamental interest both to the engineer and the physiologist. One

† Present address: Union Carbide Corporation, Bound Brook, New Jersey 08805.

frequently encounters situations where biological cells come in contact with relatively inelastic boundaries (micropipette experiments with red cells, entrance of red and white cells in capillaries and microscopic slide preparations of single cells) or with each other (consolidation of soft tissue, the centrifuging of cellular preparations and the formation of red-cell rouleaux), where the fluid film adjacent to the membrane experiences a time-dependent draining. On a larger scale this phenomenon is seen when one inserts a soft contact lens on the relatively inelastic corneal surface. Four related engineering applications include a large bubble rising owing to buoyancy against a solid boundary, a thin-walled balloon tire resting on an air or fluid film or a balloon settling on a solid surface, and the gravitational motion of small particles and droplets towards a deformable fluid–liquid interface.

While there has been no previous theory that specifically examines the time-dependent draining of a fluid film beneath membrane-bound fluid cells that support negligible bending moments, there is extensive literature on the time-dependent squeezing of a fluid film between linearly elastic surfaces, the steady-state deformation of these surfaces when in relative motion, and the draining of fluid films adjacent to deformable fluid–liquid interfaces.

The first paper to analyse rigorously the transient elastohydrodynamic interaction encountered in the normal approach of elastic solids separated by a lubricating film is attributed to Christensen (1962). In this work the elastic solids were circular cylinders and the approach was along a line joining their centres. Such motion is frequently encountered in gears and rotating machine elements. The displacement of the elastic surface is linearly related to local pressure between elastic elements. Lee & Cheng (1973) improved on Christensen's theory by removing the numerical convergence difficulties at small film thicknesses and incorporating the effect of deformation rate. Both papers deal with the hard elastohydrodynamic range (where elastic modulus of materials are sufficiently high that the lubricant pressures developed within the lubricating layer are large enough to alter the lubricant viscosity substantially). A more recent paper by Rohde, Whicker & Browne (1976) treats the problem of elastohydrodynamic squeeze films in the soft range, where large deformations occur at low lubricant pressures. In the latter paper the deformation of the elastic element is also linearly related to the local pressure. Christensen's original work in the hard elastohydrodynamic range was extended in two other papers (Christensen 1970; Herrebrugh 1970), while the treatment of the soft range has received more recent attention (Gaman, Higginson & Norman 1974; Roberts 1974; Browne, Whicker & Rohde 1975; Whicker, Browne & Rohde 1976).

The steady-state hydrodynamic deformation of elastic or fluid-filled bodies separated by a fluid film has been widely studied in connection with the theory of compliant surface bearings (Dowson & Higginson 1960; Castelli, Rightmire & Fuller 1967; Benjamin 1969), the passage of bubbles and fluid droplets through tubes (Bretherton 1961; Davis & Taylor 1949; Goldsmith & Mason 1962; Cox 1962; Hyman & Skalak 1970) and the motion of red cells through capillaries (Prothero & Burton 1961, 1962; Barnard, Lopez & Hellums 1968; Lee & Fung 1969; Hochmuth, Marple & Sutera 1970; Sutera *et al.* 1970; Seshadri *et al.* 1970; Lin, Lopez & Hellums 1973). We shall describe further the two latter applications since the modelling of the fluid cell is directly related to the present study. Membrane-bound fluid cells have been alternatively modelled as elastic pellets, liquid droplets or fluid-filled sacs whose membranes

do not support bending moments. In the first treatment Lighthill (1968) and Fitz-Gerald (1969) examined the steady-state parallel motion of an elastic pellet through a closely fitting fluid-filled tube. These papers were the first to attempt to predict the deformation of a red cell as it passes through a capillary whose dimensions are of the same order or smaller than the undeformed red cell. The deformation of the pellet is assumed to be a linear function of local film pressure, as assumed in the previously mentioned elastohydrodynamic squeeze-film studies. More recently Tözeren & Skalak (1979) have examined the Lighthill and Fitz-Gerald analysis to correct for the pressure singularity that occurs in the vicinity of the point of minimum gap width, and have applied this improved theory to model the motion of white cells translating along the axis of a tube (Tözeren & Skalak 1978). The elastic deformations are of order five per cent to ensure the validity of the linear theory of elasticity. The validity of a linear deformation law for red cells has been critically questioned (Lee & Fung 1969; Skalak 1972), since the thin-walled red-cell membrane does not support significant membrane-bending stresses and is filled with an incompressible fluid.

A more appropriate model for the deformation of a highly deformable fluid-filled membrane-bound body is one where the instantaneous shape is related to the local variations in membrane tension and curvature, and membrane-bending moments can be neglected. In this context, previous studies of the deformation of a bubble or liquid droplet interacting with a boundary in the creeping-motion regime are of interest. Bretherton (1961) has modelled the pressure-induced deformation of a bubble translating along the axis of a rigid tube. Hyman & Skalak (1970) have similarly developed a model for a periodic array of bubbles moving along the axis of a tube in the low-Reynolds-number limit. In both these studies the flow is steady, the surface tension is constant and one seeks a single steady-state equilibrium configuration for the shape of the deformed bubble. These surface-tension problems in bubble dynamics differ from membrane-bound bodies in that there is a continuity of tangential stress at the interface. The treatment of the membrane that most closely parallels the present analysis is the study by Barnard *et al.* (1968). These authors modelled the red cell in a capillary as a membrane-bound fluid with negligible bending resistance. The steady-state membrane shape was obtained by allowing the pressure difference across the membrane to be taken up by local variations in tension and curvature. Unlike the surface-tension problem for bubbles, the membrane tension is not constant but is allowed to vary as a function of the integrated fluid shearing stress on the cell surface.

There have been numerous theoretical and experimental investigations of the draining of a fluid film in foam and emulsion systems and in studies of droplet coalescence.† Princen (1963) determined the outer solution for the contact angle of a spherical droplet resting under its own weight at a fluid–liquid interface. Most relevant to the present theoretical model are the studies of Hartland (1967, 1968, 1969), Jones & Wilson (1978) and Dimitrov & Ivanov (1978) on the approach of a spherical particle or droplet to a fluid–liquid interface. In these problems the interface deforms to lowest order to the shape of the particle or droplet and establishes a thin lubricating layer in which the local pressure forces driving the fluid in the film are balanced by small changes in the tension–curvature relation for the interface. As first demonstrated by Hartland the long-time draining of the film is associated with a trapping of fluid in

† The authors wish to thank one of the referees for bringing this literature on fluid–liquid interfaces to their attention.

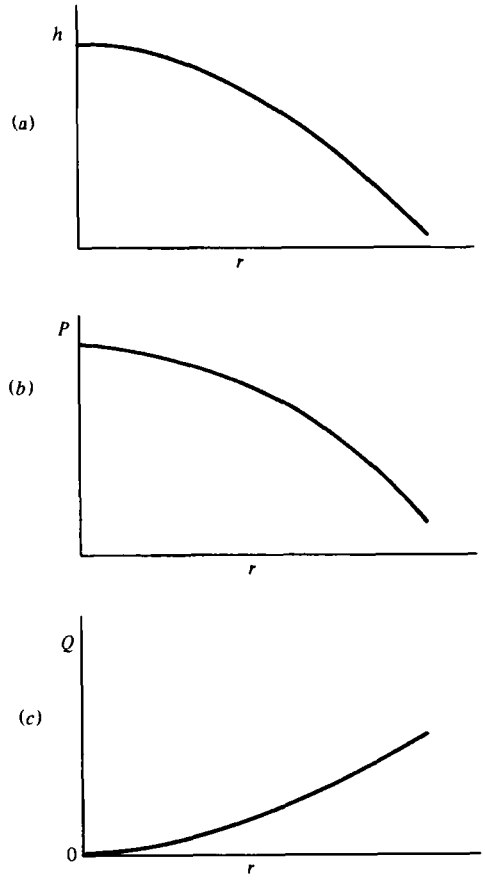

FIGURE 1. Schematic representation of the spatial distribution of variables for elastohydrodynamic squeeze-film theory: (*a*) h *vs.* r; (*b*) P *vs.* r; (*c*) Q *vs.* r.

the inner region of the film caused by the formation of a narrow fluid gap near the edge of the near-contact area. The fluid flow through the edge region and the shape of the gap adjust such that at each instant in time the pressure drop between the inner region of trapped fluid and the lower-pressure external fluid just balances the viscous losses in the gap. The basic long-time behaviour is qualitatively the same whether the flow in the gap is a plug flow corresponding to two fluid interfaces, with a continuity of shearing stress at each interface, or a parabolic profile for a solid surface and one interface. The boundary conditions for the latter problem are the same as for the fluid film between two abutting membrane-bound fluid cells in the present paper. The paper by Jones & Wilson uses the same asymptotic large-time approximation introduced in §2.3, although the authors were not aware of this earlier analysis and that closed-form expressions could be derived for the drainage rate. While the fluid-trapping phenomenon has been known for more than a decade, the initial-value problem describing the detailed sequence of events leading to the quasi-steady trapping configuration is still largely unknown. The solution to this problem, which occurs during the very early stages of the film drainage, is the principal objective of the present investigation.

Although the deformation of the elastic solid in elastohydrodynamic squeeze-film theory is somewhat similar to the early-time deformation of the membrane in the

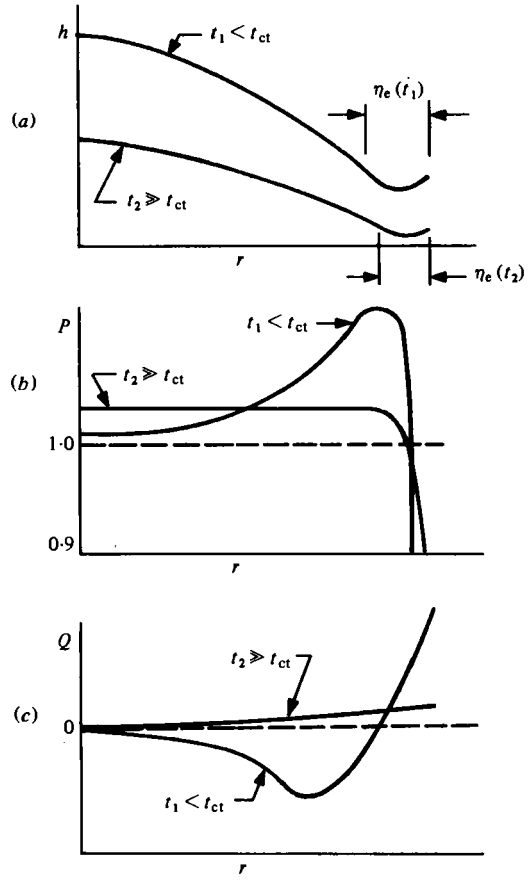

FIGURE 2. As figure 1, but for membrane squeeze-film theory.

membrane squeeze-film theory in this work, there is an intriguingly different behaviour for both the pressure and flow fields during the early stages of the development of the lubricating film. Curiously, the pressure distribution and flow behaviour for the elastohydrodynamic film qualitatively parallels the membrane squeeze films for large times when the shape of the inner region is significantly different. Figures 1 and 2 are schematic illustrations comparing qualitatively the film thickness h, pressure P and volume flow rate Q in elastohydrodynamic and membrane squeeze-film theory. Figures 1 (a–c) show typical profiles obtained in elastohydrodynamic squeeze film theory at small film thicknesses for the case where the indenter is a circular cylinder whose planar front surface approaches another planar surface with an intervening fluid film. As seen from figures 1 (a, b) the maximum pressure occurs at the point of maximum film thickness. Figure 1 (c) shows a positive outward flow rate increasing with distance from the origin. Figures 2 (a–c) are qualitative sketches for the same variables, as predicted by the membrane squeeze-film theory presented herein, where the membrane-bound body is initially an axisymmetric shape similar to an applanated fluid cell. Two sets of curves are shown, $t_1 < t_{ct}$ and $t_2 \gg t_{ct}$, where t_{ct} is the characteristic time to trap fluid in the inner region of the near-contact area. For the membrane squeeze-film theory a pressure maximum quickly forms ($t \ll t_{ct}$) near the edge of the near-contact area and there is flow inward from this point. The curves for $t_1 < t_{ct}$ in

figures 2(*a–c*) are representative profiles for the timescale t_{ct} during which the edge region is established and the fluid trapping occurs. As time increases, the pressure peak near the edge region eventually disappears and the inflow of the fluid will vanish. For large times $t_2 \gg t_{ct}$ the pressure peak associated with the fluid trapping is replaced by a pressure plateau in the central region and a monotonically decreasing pressure in the edge region. This pressure profile produces an outward positive volume flow rate for all radii which slowly drains the trapped fluid in the interior on a much longer timescale, as shown by Hartland. The two geometric parameters of importance for fluid cells are the radius of the near-contact area and the radius of curvature of the static outer region. Numerical solutions are obtained for various aspect ratios of the radius of curvature of the static outer region to the radius of the near-contact area.

The formulation of the theoretical problem is presented in §2. An order-of-magnitude analysis is performed in §2.1, which deduces the two characteristic times for the membrane-deformation and fluid-draining behaviour. The motivation for the inner- and edge-region approximations is an outcome of this order-of-magnitude analysis. The treatment of the edge region is discussed in §§2.2 and 2.3. A description of the numerical solution procedure is given in §2.4, while §3 discusses the results. In §4 an experiment confirming the bidirectional flow behaviour during the early period following the application of the load is discussed.

2. Formulation

Consider the transverse motion of the membrane boundary of a fluid-filled cell that squeezes out the fluid film adjacent to a rigid planar surface. A constant load F is impulsively applied to the cell's upper surface, as shown in figure 3, which induces a uniform pressure P_c both inside the cell and initially in the fluid film.† The difference in pressure across the membrane is related to the membrane tension and local membrane curvature that result from the motion of the fluid after the initial loading. The initial shape for the cell is an axisymmetric body with a plane boundary, parallel to the rigid surface, and a circular edge (much like a balloon squeezed between parallel plates).‡ The initial film thickness $h(r, 0)$ is thus assumed constant and chosen to be two or more orders of magnitude smaller than the cell radius.

† The initial pressure and film-thickness profile for a bubble or liquid droplet moving toward a fluid–liquid interface and an impulsively loaded cell differ substantially. For the impulsively loaded cell the pressure in the fluid film at the origin instantly rises to the cell pressure and the membrane curvature vanishes. The membrane applanates radially and the fluid is expelled by the steep pressure gradient at the edge of the expanding near-contact area. This process stops when the applied load F is equal to $p_c A$, where A is the near-contact area after the loading is completed. The initial profile after loading is a top-hat function with a uniform initial thickness equal to the film thickness at the origin when the load is applied. This behaviour is easily observed in the simple balloon experiment described at the end of the paper. For a small bubble or liquid drop moving toward a boundary under the influence of gravity the droplet–film interface evolves as a slow departure from an initially spherical shape.

‡ For a non-distensible membrane the cell geometry before loading is either that of a finite disk with rounded edges or a circular bag formed from two planar sheets that are sealed at their edges. It cannot be a spherical shell since this would buckle inward forming a spherical dimple with negligible tension in the interior and a hoop tension along the ring of contact. For a highly distensible membrane, such as a rubber balloon, the initial shape can be spherical. Here we shall require that the incremental deformation in the applanated area be small compared with the initial stretching of the membrane due to its inflation. Under these conditions the membrane tension in the near-contact area will be nearly uniform.

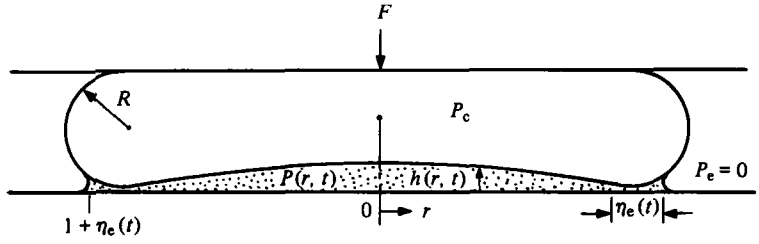

FIGURE 3. Geometry for the membrane squeeze-film theory.

For a film thickness h that is two or more orders of magnitude smaller than the near-contact radius a and a vorticity diffusion time h^2/ν that is much less than the characteristic time for the draining of the film, the flow field may be assumed quasi-steady with a temporally and spatially varying film thickness. The fluid film is regarded as incompressible and radially symmetric so that the continuity and radial momentum equations are

$$\frac{1}{r}\frac{\partial ur}{\partial r}+\frac{\partial w}{\partial z}=0, \tag{2.1}$$

$$\frac{1}{\mu}\frac{\partial P}{\partial r}=\nabla^2 u-\frac{u}{r^2}, \tag{2.2a}$$

where P is the fluid pressure, u and w are the fluid velocity components in the radial and axial directions respectively, and μ is the fluid viscosity.

If the term u/r^2 in (2.2a) is replaced by its expression from (2.1) and the approximations made that $w \ll u$ and $\partial/\partial r \ll \partial/\partial z$ in the resulting expression for the viscous stress, one obtains

$$\frac{1}{\mu}\frac{\partial P}{\partial r}=\frac{\partial^2 u}{\partial z^2}. \tag{2.2b}$$

Similarly, for the axial component of the momentum equation we assume that the fluid pressure is constant across the film thickness:

$$\frac{\partial P}{\partial z}=0. \tag{2.3}$$

According to (2.3) pressure is not a function of z, so that the velocity u may be obtained by integrating (2.2b) twice. Applying the no-slip boundary condition at the planar surface $z = 0$ and at the membrane boundary $z = h(r,t)$ yields

$$u=\frac{1}{2\mu}\frac{\partial P}{\partial r}[z^2-zh(r,t)], \tag{2.4a}$$

where $h(r,t)$ is the time-dependent film thickness. For the problem of two cells squeezing out a fluid film between them, with the midplane between cells at $z = 0$ and $\frac{1}{2}h$ the distance from midplane to either cell, the equivalent expression to (2.4a) that satisfies the symmetry condition at $z = 0$ yields

$$u=\frac{1}{2\mu}\frac{\partial P}{\partial r}[z^2-\tfrac{1}{4}h^2(r,t)]. \tag{2.4b}$$

The flow rate Q is obtained by integrating (2.4a) or (2.4b) over the area normal to the flow direction. Equations (2.4a) and (2.4b) give the same results for the flow rate:

$$Q = -\frac{\pi}{6\mu} r \frac{\partial P}{\partial r} h^3(r,t). \tag{2.5a}$$

If the membrane-bound cell were replaced by a large bubble pressing against a rigid planar surface perpendicular to the direction of gravity the no-slip boundary condition at the interface would be replaced by

$$\left.\frac{\partial u}{\partial z}\right|_{z=h(r,t)} = 0,$$

if the viscosity of the air was neglected. Equation (2.5a) would then be replaced by

$$Q = -\frac{2\pi}{3\mu} r \frac{\partial P}{\partial r} h^3(r,t). \tag{2.5b}$$

The continuity equation (2.1), when multiplied by $2\pi r$ and integrated across the film thickness, gives

$$2\pi \int_0^{h(r,t)} \frac{\partial ur}{\partial r}\, dz = -2\pi r w(h). \tag{2.6a}$$

Applying the Leibnitz rule for differentiating an integral with variable limits, introducing the definition of Q and replacing the fluid velocity $w(h)$ by the local membrane velocity $\partial h/\partial t$, one has

$$\frac{\partial Q}{\partial r} = -2\pi r \frac{\partial h}{\partial t}. \tag{2.6b}$$

The tangential force balance in the plane of the membrane in the near-contact area requires an equilibrium between the fluid shearing stress τ in the radial direction and the membrane tensions σ_r and σ_θ in the radial and azimuthal directions:

$$r\tau = \frac{\partial(\sigma_r r)}{\partial r} - \sigma_\theta. \tag{2.7a}$$

For a fluid cell whose initial geometry conforms to one of the configurations described in the footnote at the beginning of this section, it is reasonable to assume that the membrane tension after loading is isotropic in the near-contact area, that is

$$\sigma_r = \sigma_\theta = \sigma.\dagger$$

Also the fluid shearing stress can be simply related to the fluid-film pressure by taking a force balance on a cylindrical fluid shell of thickness dr whose height varies as the local film thickness. Equation (2.7a) becomes

$$\frac{\partial \sigma}{\partial r} = \tfrac{1}{2} h \frac{\partial p}{\partial r}. \tag{2.7b}$$

The normal force balance for a membrane undergoing small deformations which offers no bending resistance but is subjected to an isotropic tensile stress produced

† Note that σ is not constant beyond the edge of the near-contact area, but varies in accordance with Laplace's law with two finite orthogonal radii of curvature. In the near-contact region the membrane is similar to an isotropic tension membrane on a circular drum.

by a distributed axisymmetric pressure loading can be written as (see e.g. Hildebrand 1976, p. 459)

$$\sigma \frac{\partial}{\partial r}\left(r\frac{\partial h}{\partial r}\right) = r(P_c - P), \tag{2.8}$$

where P_c is the uniform internal cell pressure and $P(r,t)$ is the instantaneous local film pressure. Equation (2.8) is valid for arbitrary axisymmetric small-amplitude membrane deflections in which inertia effects are negligible.

Equations (2.5)–(2.8) differ from the formulation of elastohydrodynamic squeeze-film theory (Christensen 1962; Rohde *et al.* 1976) in that (2.7) and (2.8) relating the pressure and membrane tension replace the pressure-induced elastic-deformation relation for a linearly elastic solid. Equations (2.5)–(2.8) provide four coupled non-linear equations for Q, P, σ and h.

The boundary conditions on (2.5)–(2.8) are

$$\frac{\partial h(0,t)}{\partial r} = 0, \quad Q(0,t) = 0, \tag{2.9a, b}$$

$$P(a,t) = P_e, \quad \frac{\partial^2 h(a,t)}{\partial r^2} = \frac{1}{R}, \tag{2.9c, d}$$

$$\sigma(a,t) = \sigma_e = (P_c - P_e)R, \tag{2.9e}$$

where a is the radius of the near-contact area, P_e the constant exit pressure, R is the constant radius of curvature of the static outer region and σ_e is the membrane tension at the edge of the near-contact area.

The boundary condition (2.9*a*) is the symmetry condition of the highly flexible membrane, and (2.9*b*) represents the vanishing flow rate at the origin of the lubricating film. The pressure boundary condition at $r = a$ (2.9*c*) requires the film pressure to reach the value of the constant exit pressure at the edge of the cell. The boundary conditions (2.9*d–e*) represent the requirements that the membrane returns to the curvature of the static outer edge and the membrane tension be continuous with the tension developed in the static outer edge. Equation (2.9*e*) is Laplace's law applied at the edge of the near-contact area where the radius of curvature in the azimuthal plane normal to the membrane is assumed to be much larger than R. The initial condition is

$$h(r,0) = h_0. \tag{2.9f}$$

This is a suitable initial condition for an impulsive loading of the cell where the initial thickness distribution is nearly uniform.

To simplify the boundary-value problem defined by (2.5)–(2.8) and the boundary conditions (2.9) we shall first perform an order-of-magnitude analysis to identify the important time- and lengthscales in the problem.

2.1. *Order-of-magnitude analysis*

For a cell that has an edge radius of curvature R, the tension force σ is of order $(P_c - P_e)R$, where P_e is the constant exit pressure, taken to be zero. As discussed in § 1 two different time- and streamwise lengthscales characterize the draining of the near-contact area. The two streamwise lengthscales are the radius a of the near-contact area, which is also the characteristic length of the central region of the film, and the

characteristic length η of the edge region. Since the pressure difference across the edge region is of order p_c and the tension force is of order $p_c R$, one concludes from (2.8b) that if $\partial^2 h/\partial r^2$ is approximated by h/η^2 then

$$\eta \sim O((Rh)^{\frac{1}{2}}). \tag{2.10}$$

The pressure driving force that is felt across the edge region is of order p_c on both the short and long timescales. The principal difference, as illustrated in figure 2, is that on the short timescale there is a non-vanishing negative pressure gradient in the central region as opposed to the pressure plateau that is established for large time. From (2.5b) the flow through the edge region is of order

$$Q = O\left(\beta a p_c \frac{h^3}{\eta}\right), \tag{2.11}$$

where $\beta = \pi/6\mu$. During the early-time period, h in the edge region is of the order of the initial thickness h_0, which in general is much larger than the edge-region film thickness h_e after fluid trapping has occurred. Combining (2.10) and (2.11), one concludes that Q is proportional to $h^{\frac{5}{2}}$.

We shall first deduce the characteristic time for the collapse of the edge region. Since the flow bifurcates about the pressure maximum, Q is zero at the maximum, which lies just interior to the $p = p_c$ location, and the radial gradient of the flow in the edge region is of order Q/η. From (2.6b) the characteristic time t_{ct} for the edge-region formation is

$$t_{ct} = O\left(\frac{a h_0 \eta}{Q}\right). \tag{2.12}$$

Substituting (2.10) and (2.11) for η and Q into (2.12), one obtains

$$t_{ct} = O\left(\frac{R}{\beta p_c h_0}\right) = O\left(\frac{\eta^2}{\beta p_c h_0^2}\right). \tag{2.13}$$

To gain understanding of the meaning of (2.13) consider a rigid plate with a flat blunt edge of thickness η approaching a planar surface separated by a fluid film of thickness h_0. The fluid is drained from the gap by pushing the blunt-edged plate with a constant force F per unit width toward the planar surface. The average pressure p_c on the edge of the plate is given by F/η. One can easily show for this rigid geometry that the characteristic time for the draining of the film is

$$t_p = O\left(\frac{\eta^2}{\beta p_c h_0^2}\right), \tag{2.14}$$

which is the same as (2.13). One concludes that the collapse of the edge region behaves very much as if the edge of the near-contact area were a two-dimensional rigid indenter.

Let us now deduce the characteristic time for the draining of the trapped fluid in the central region of the film. The flow Q through the edge region is now not generated by its own collapse, but by the drainage of fluid in the interior. The flow gradient in the central region is of order Q/a. From (2.6b) the characteristic time t_{cd} for draining the central region is

$$t_{cd} = O\left(\frac{a^2 h_0}{Q}\right), \tag{2.15}$$

where h_0 is now the thickness of the central region of the film. Substituting (2.11) in (2.15), one has

$$t_{cd} = O\left(\frac{ah_0\eta}{\beta p_c h_e^3}\right) = O\left(\frac{ah_0 R^{\frac{1}{2}}}{\beta p_c h_e^{\frac{5}{2}}}\right), \tag{2.16}$$

where h in (2.11) is now the collapsed edge height h_e. The ratio of the draining time (2.16) to the trapping time (2.12) is of order $ah_0^3/\eta h_e^3$. In the numerical computations presented later in this paper this ratio is of order 10^3 or larger.

Implicit in the foregoing order-of-magnitude analysis is the assumption that the fluid shearing stresses are a higher-order correction to the membrane tension. From (2.7*b*) $\partial\sigma/\partial r$ is of order $h_0 p_c/a$ in the central region and order $h_e p_c/\eta$ in the edge region. Introducing the characteristic length (2.10) for η in the latter expression, one concludes that the edge-region tension gradient is of order $(h_e/R)^{\frac{1}{2}}$. Thus in either case the membrane tension is uniform to lowest order in the near-contact area. Thus (2.7*b*) will be approximated by

$$\frac{\partial\sigma}{\partial r} = 0 \quad (r < a), \tag{2.17}$$

where σ is given by its value determined from the edge condition (2.9*c*). To this same order (2.8) will be approximated by

$$\sigma_e \frac{\partial}{\partial r}\left(r\frac{\partial h}{\partial r}\right) = r(P_c - P). \tag{2.18}$$

The approximation (2.17) thus reduces the problem to the solution of (2.5*a*), (2.6) and (2.18) for the variables h, P and Q.

The existence of a small region in which the pressure is changing rapidly and a considerably larger region in which the variables are changing slowly is conducive to a two-region approximation of the near-contact area. The full non-dimensionalized form of (2.5*a*), (2.6) and (2.18) will be solved for the inner region, whereas for the smaller edge region an approximate integral formulation will be developed.

Equations (2.5*a*), (2.6) and (2.18) are now non-dimensionalized using the following definitions:

$$r^* = \frac{r}{a}, \quad h^* = \frac{h}{a}, \tag{2.19a, b}$$

$$P^* = \frac{P - P_e}{P_c - P_e}, \quad \sigma^* = \frac{\sigma}{(P_c - P_e)R}, \quad Rl^* = \frac{R}{a}, \tag{2.19c, d, e}$$

$$Q^* = \frac{Q}{\beta a^3 (P_c - P_e)}, \quad T^* = \frac{t}{1/\beta(P_c - P_e)}. \tag{2.19f, g}$$

If one drops the * notation, for convenience, the non-dimensional equations are

$$Q = -r\frac{\partial P}{\partial r}h^3, \tag{2.20a}$$

$$\frac{\partial Q}{\partial r} = -2\pi r\frac{\partial h}{\partial T}, \tag{2.21a}$$

$$r(1-P) = Rl\frac{\partial}{\partial r}\left(r\frac{\partial h}{\partial r}\right), \tag{2.22a}$$

where Rl is the non-dimensional aspect ratio of the cell (ratio of radius of curvature of the outer region to radius of the near-contact area).

The beginning of the edge region is arbitrarily chosen as the unknown location where $P = 1$. This choice is convenient since the left-hand side of (2.22a) vanishes at this location and thus provides convenient matching conditions for the edge profile. The inner region is the bulk of the near-contact region and terminates at $r = 1-\eta_e(T)$, where $\eta_e(T)$ is the time-dependent edge-region size. This inner-region–edge-region interface is approximated to be at $r = 1$ on the inner lengthscale because the computer program for the numerical solution of the inner region requires a fixed length. This approximation is consistent with the method of asymptotic expansions, where the larger scale is kept constant and the smaller scale is allowed to vary. The boundary and matching conditions for the inner region are

$$\frac{\partial h(0,T)}{\partial r} = 0, \quad h(1,T) = H_0(T), \tag{2.23a, b}$$

$$P(1,T) = 1, \quad Q(0,T) = 0. \tag{2.23c, d}$$

The initial conditions are

$$H(r,0) = \epsilon, \quad P(r,0) = 1, \tag{2.24a, b}$$

$$Q(r,0) = 0, \quad H_0(0) = \epsilon, \tag{2.24c, d}$$

where $H_0(T)$ is the time-dependent film thickness at the interface of the two regions. The value of $H_0(T)$ is obtained by matching the solutions from the inner and edge regions at each instant in time.

2.2. *Treatment of the edge region*

For the edge region (figure 4) a new coordinate η is defined as

$$\eta = r-1 \quad (1 \leqslant r \leqslant 1+\eta_e(T)). \tag{2.25}$$

Using the above definition, the governing equations (2.20a), (2.21a) and (2.22a) may be rewritten as

$$Q(\eta,T) = -(1+\eta)\frac{\partial P}{\partial r}h^3(\eta,T), \tag{2.20b}$$

$$\frac{\partial Q}{\partial \eta} = -2\pi(1+\eta)\frac{\partial h}{\partial T}, \tag{2.21b}$$

$$(1+\eta)(1-P) = Rl\frac{\partial}{\partial \eta}\left[(1+\eta)\frac{\partial h}{\partial \eta}\right]. \tag{2.22b}$$

The mathematical description of the edge region can be simplified by using an approximate integral formulation. A polynomial profile for pressure is assumed in the edge region,

$$P(\eta,T) = C_1+C_2\eta+C_3\eta^2, \tag{2.26}$$

which satisfies the following matching and boundary conditions:

$$P(0,T) = 1, \quad \frac{\partial P(0,T)}{\partial r} = P_{0\eta}(T), \tag{2.27a, b}$$

$$P(\eta_e(T),T) = 0, \tag{2.27c}$$

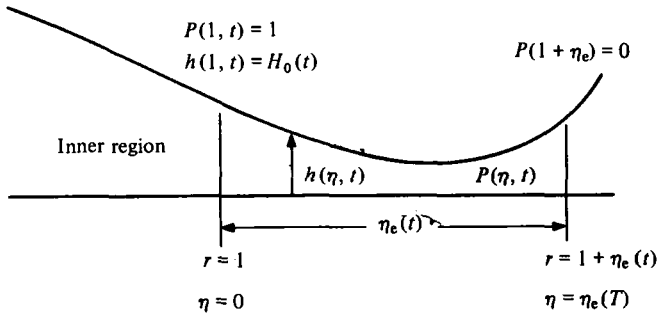

FIGURE 4. Geometry for the edge region of the near-contact area.

where $P_{0\eta}(T)$ is the pressure gradient at the interface of the two regions obtained from the inner-region solution at $r = 1$. The resulting expression for $P(\eta, T)$ is given by

$$P(\eta, T) = 1 + P_{0\eta}(T)\eta - \gamma(T)\eta^2, \tag{2.28}$$

where

$$\gamma(T) = \frac{1 + P_{0\eta}(T)\sigma_e(T)}{\eta_e^2(T)} \tag{2.29}$$

The membrane profile in the edge region is obtained by integrating the normal force-balance equation (2.22*b*) twice using the pressure profile from (2.28). The resulting expression contains two coefficients, which are found by using the following interface matching conditions:

$$h(r = 1, T) = H_0(T) = h(\eta = 0, T), \tag{2.30a}$$

$$\frac{\partial h(r = 1, T)}{\partial r} = H_{0\eta}(T) = \frac{\partial h(\eta = 0, T)}{\partial \eta}, \tag{2.30b}$$

where $H_0(T)$ is the interface-film thickness and $H_{0\eta}(T)$ is the membrane slope at the interface. The edge-region membrane profile can then be written as

$$\begin{aligned} h(\eta, T) = {} & H_0(T) + H_{0\eta}(T)\ln(1+\eta) \\ & + \frac{P_{0\eta}(T)}{Rl}[\tfrac{1}{6}\eta^3 + \tfrac{1}{12}\eta^2 - \tfrac{1}{6}\eta + \tfrac{1}{6}\ln(1+\eta)] \\ & - \frac{\gamma(T)}{Rl}[\tfrac{1}{16}\eta^4 + \tfrac{1}{36}\eta^3 - \tfrac{1}{24}\eta^2 + \tfrac{1}{12}\eta - \tfrac{1}{12}\ln(1+\eta)]. \end{aligned} \tag{2.31a}$$

Using a Taylor-series expansion for $\ln(1+\eta)$, where $\eta \ll 1$, (2.31*a*) may be approximated by

$$h(\eta, T) = H_0(T) + H_{0\eta}(T)[\eta - \tfrac{1}{2}\eta^2] - \frac{P_{0\eta}(T)}{Rl}[\tfrac{1}{6}\eta^3 - \tfrac{1}{24}\eta^4] + \frac{\gamma(T)}{Rl}(\tfrac{1}{12}\eta^4 - \tfrac{1}{5}\eta^5). \tag{2.31b}$$

Since $\eta \ll 1$ the local membrane velocity in the edge region is approximated by (neglecting terms of order η^2 or higher)

$$\frac{\partial h}{\partial T} = \dot{H}_0(T) + \dot{H}_{0\eta}(T)\eta. \tag{2.32}$$

The volume-flow-rate distribution in the edge-region film may be obtained by integrating the continuity equation (2.21*b*) and using the result of (2.32):

$$Q(\eta, T) = Q_0(T) - 2\pi\dot{H}_0(T)\,[\eta + \tfrac{1}{2}\eta^2] - 2\pi\dot{H}_{0\eta}(T)\,[\tfrac{1}{2}\eta^2 + \tfrac{1}{3}\eta^3], \tag{2.33}$$

where the value of the interface volume flow rate evaluated at $r = 1, Q_0(T)$ is obtained from the solution of the inner region.

The momentum equation (2.20*b*) is now satisfied in integral form. Substituting (2.33) into (2.20*b*), integrating the latter across the edge region and applying the pressure boundary conditions (2.27*a*, *c*), one finds

$$1 = -2\pi\dot{H}_0 I_1 + Q_0 I_2 - 2\pi\dot{H}_{0\eta} I_3, \tag{2.34}$$

where

$$I_1 = \int_0^{\eta_e(T)} \frac{(\eta + \frac{1}{2}\eta^2)\,d\eta}{(1+\eta)\,h^3(\eta, T)}, \tag{2.35a}$$

$$I_2 = \int_0^{\eta_e(T)} \frac{d\eta}{(1+\eta)\,h^3(\eta, T)}, \tag{2.35b}$$

$$I_3 = \int_0^{\eta_e(T)} \frac{(\frac{1}{2}\eta^2 + \frac{1}{3}\eta^3)\,d\eta}{(1+\eta)\,h^3(\eta, T)}. \tag{2.35c}$$

Equation (2.34) is treated numerically as an ordinary differential equation to determine $H_0(T)$, with instantaneous values of $Q_0(T)$ and $\dot{H}_{0\eta}(T)$ considered known from the inner-region solution at $r = 1$ evaluated at the previous time step.

At this point the value of $\eta_e(T)$ is not known but can be obtained by requiring that the momentum equation (2.20*b*) be satisfied exactly at $\eta = \eta_e(T)$. This has the effect of ensuring that the pressure gradient at the edge-region exit provides a volume flux that is compatible with the expression (2.33) evaluated at η_e. Substituting the relation for the unknown interface-membrane velocity $\dot{H}_0(T)$ from (2.34) into (2.33) and inserting the latter into (2.20*b*), one obtains

$$Q_0(T) - 2\pi\dot{H}_{0\eta}(T)\,[\tfrac{1}{2}\eta_e^2(T) + \tfrac{1}{3}\eta_e^3(T)] - \frac{\eta_e(T) + \frac{1}{2}\eta_e^2(T)}{I_1}\,[Q_0(T)\,I_2 - 1 - 2\pi\dot{H}_{0\eta}(T)\,I_3]$$
$$= [1 + \eta_e(T)]\left[P_{0\eta}(T) + \frac{2}{\eta_e(T)}\right] h_e^3(T), \tag{2.36}$$

where $h_e(T)$ is the film thickness at $\eta = \eta_e(T)$ from (2.31). Equation (2.36) is an integral equation for $\eta_e(T)$ since the limits on the integrals I_1, I_2 and I_3 defined by (2.35) are functions of $\eta_e(T)$. The solution of (2.36) at each time step is accomplished by a numerical trial-and-search procedure described in §2.4.

2.3. *Asymptotic theory for large time*

The numerical solutions presented in §3 reveal that for very large times, after the fluid-trapping phase is completed and the fluid draining is well established, the pressure plateau extends over most of the near-contact area and the volume flow through the edge region is nearly independent of position and is a slowly varying function of time. These two observations allow one to significantly simplify the description of the inner- and edge-region flows for large time, as first deduced by Jones & Wilson (1978). These authors used physical arguments to support their contention that the long-time

behaviour is insensitive to initial conditions. The asymptotic analysis in this section closely parallels that given in this last reference.

In contrast to §2.3, where the interface between the inner and edge regions was chosen for convenience to be at the radial location where P is equal to unity, we now redefine this interface to be the edge of the region where the radial pressure gradient is nearly zero. For computational purposes this is taken to be at the location where the local value of h is approximately ten times the minimum gap height, since the local pressure gradient, which varies as h^{-3}, is of order 10^{-3} less than the characteristic edge-region gradient at this point.

In view of the foregoing remarks, the large-time approximation for the inner region will neglect (2.20a) (this is equivalent to treating the trapped fluid in this region as a constant-pressure reservoir) and consider the pressure in (2.22a) as a slowly varying function of time $P_1(T)$. Equation (2.22a) can now be integrated twice and the boundary condition (2.23a) applied. The membrane displacement in the interior is given by

$$h(r,T) = h(0,T) + \frac{r^2}{4Rl}(1-P_1) \quad (r < r_1), \tag{2.37}$$

where $r_1(T)$ is the edge of the pressure plateau as defined above. Equation (2.37) is the approximation for a spherical cap in uniform loading inder constant tension. When the result (2.37) is substituted in (2.21a) and the latter integrated subject to boundary condition (2.24c), one finds

$$Q(r,T) = -\pi r^2\left(\frac{dh(0,T)}{dT} - \frac{r^2}{8Rl}\frac{dP_1}{dT}\right) \quad (r < r_1). \tag{2.38}$$

Since the volume of fluid in the edge region is very small compared with that trapped in the interior for large times, continuity considerations require that the volume flow through the edge region be nearly equal to that exiting from the interior at the interface r_1. Equation (2.21b) can therefore be replaced by the approximation

$$Q(\eta,T) = Q(r_1,T) = Q_0(T), \tag{2.39}$$

and this simplification also introduced into (2.20b). Equation (2.22b) can now be differentiated with respect to η and the expression for $\partial P/\partial\eta$ obtained from (2.20b). This leads to an ordinary differential equation for the edge-region profile:

$$(1+\eta)\frac{\partial^3 h}{\partial\eta^3} + \frac{\partial^2 h}{\partial\eta^2} - \frac{1}{1+\eta}\frac{\partial h}{\partial\eta} - \frac{Q_0(T)}{Rlh^3} = 0. \tag{2.40}$$

Equation (2.40) in the limit $\eta \ll 1$ is equivalent to equation (2.9) of Jones & Wilson (1978).

The pressure distribution in the edge region is obtained by integrating

$$-\frac{\partial P}{\partial\eta} = \frac{Q_0}{(1+\eta)h^3} \tag{2.41}$$

subject to the boundary conditions

$$P(0,T) = P_1(T) \quad (\eta = 0) \tag{2.42}$$

and (2.27). The boundary conditions for (2.40) are obtained by requiring that h and its first two derivatives be continuous at $r = r_1$ or $\eta = 0$.

Equation (2.38) when evaluated at $r = r_1$ contains two unknowns $dh(0,T)/dT$ and dP_1/dT. Since the length of the inner region varies only slightly, we shall assume for the purposes of relating $h(0,T)$ and P_1 that the projected location r_0 where the circular arc (2.37) touches the planar surface does not change with time. Thus from (2.37)

$$h(0,T) = \frac{r_0^2}{4Rl}(P_1(T) - 1). \tag{2.43}$$

When (2.43) is substituted into (2.37) the resulting expression for the film thickness h is of the form of equation (2.10) of Jones & Wilson (1978).

Substituting (2.43) into (2.38) and evaluating at r_1, one obtains:

$$Q_0(T) = -\frac{\pi r_1^2}{4Rl}(r_0^2 - \tfrac{1}{2}r_1^2)\frac{dP_1}{dT}. \tag{2.44}$$

The solution of the boundary-value problem for the coupled system of ordinary differential equations (2.40) and (2.41), where Q_0 is given by (2.44), involves split boundary conditions. Equation (2.40) is first integrated for a trial value of dP_1/dT to determine $h(\eta,T)$ and then (2.41) is integrated using this $h(\eta,T)$ distribution to the edge of the near-contact area, $r = 1$, where the edge condition (2.27) must be satisfied. Small adjustments in dP_1/dT at each time step are required for this edge condition to be satisfied exactly. The solution for dP_1/dT is then used to advance P_1 to the next time step. Equation (2.40) is now integrated using the latest value of P_1 in the boundary conditions at $\eta = 0$ and a new trial-and-search routine started for dP_1/dT.

2.4. *Numerical solution procedure*

The Rayleigh–Ritz–Galerkin method is used for spatial discretization of the inner region, and the solutions for the dependent variables are composed of a series of B-splines between spatial mesh points. This is accomplished with a partial-differential-equation code available from Bell Laboratories. The code package is called POST, and with the addition of supporting subroutines the solution of the ordinary differential equation (2.34) may be used as a boundary condition at the interface between the inner and edge regions. A detailed discussion of the code package appears in Schryer (1977).

To start the numerical procedure the initial conditions (2.24) are set for the variables h, P, Q and H_0. For the first few time steps the value of $\eta_e(T)$ is held constant owing to the singularity of (2.36) for $\eta = 0$. The value chosen for η_e during this early period was arbitrarily chosen to be of order ϵ. The edge-region size grows in time from its initial value to the characteristic size given by (2.16). Following this start-up period (2.36) is interrogated at each time step to determine $\eta_e(T)$.

A typical iteration in time is advanced through (2.21a). Having established a new distribution for $h(r,T)$, (2.20a) and (2.22a) are used to solve for the inner-region distributions of P and Q, subject to the boundary and matching condition (2.23). In order to satisfy the condition (2.23b) a subroutine containing the ordinary differential equation (2.34) is called. In this subroutine tentative values for $\partial h/\partial r$, Q, $\partial P/\partial r$ and $\dot{H}_{0\eta}$ at $r = 1$ are stored for use in determining $\eta_e(T)$ for this iteration. Having computed a tentative value for $\eta_e(T)$ the numerical program evaluates the definite integrals, given by (2.35a–c), and (2.34) is solved for $H_0(T)$.

A comparison is made between the interface value of h obtained from the inner-region solution and from the ordinary differential equation (2.34). If agreement does

not meet the accuracy requirement imposed on the solution of all the variables the tentative time step is reduced and the iteration procedure is begun anew. When the accuracy requirement is met the time step is said to have been successful and the first iteration of the next time iteration is begun.

Typically twenty or more evaluations of (2.34) are required for convergence on a successful time step in the early period of the numerical solution, and as few as three evaluations are required at large times. After the tolerances on the dependent variables have been met the edge-region distributions are solved for use in (2.28), (2.31) and (2.33).

The numerical solution of the fluid-trapping phase requires approximately 30 min of computation time. The numerical solution to describe the long-time draining of the trapped fluid to roughly 30 % of its initial thickness at the origin takes approximately 2 hours of IBM-370 computing time for a cell with an aspect ratio equal to 2·0. For decreasing values of the aspect ratio the computing time required to obtain a given degree of membrane collapse increases. The large amount of computer time is due to the complexity of the POST code package for solving the partial differential equations in the inner region of the near-contact area and the large differences in timescales of the fluid-trapping and draining phases of the motion. One observes from the results that the very-long-time asymptotic analysis developed in §2.3 becomes valid for characteristic times that are roughly two orders of magnitude larger than the time required for the film thickness at the origin to have achieved its maximum value. At this time the uniform pressure plateau extends to nearly 90 % of the near-contact area, and the edge-region approximation for Q in §2.3 is closely approached. The POST routine is now discarded and the changeover to the asymptotic solution procedure implemented.

3. Results and discussion

The solutions to the governing equations developed in §2 are presented in non-dimensional form. The spatial variable r is renormalized with respect to the entire near-contact radius $1+\eta_e(T)$. This renormalization allows the change in interface location to be viewed from the perspective of a constant near-contact radius. Since time is normalized with respect to the fluid viscosity and the pressure difference across the outer-region membrane, the solutions at a given time may be compared for each case to see the influence that the cell's aspect ratio Rl has on the draining behaviour of the fluid film. The dimensionless initial film thickness ϵ used for all of the numerical solutions is equal to 10^{-2} because this magnitude is representative of the film thicknesses seen in the applications mentioned earlier. Results for three values of the aspect ratio Rl, varying from 0·25 to 2·0, are presented herein. Additional numerical results can be found in Wu (1981).

The graphs in figures 5 (*a–c*) show the solutions for the time-varying film thickness between a rigid planar surface and a membrane-bound cell with the aspect ratios 2·0, 0·75 and 0·25. The solid dot on each curve in these figures indicates the location of the matching interface where $P = 1$. To obtain the membrane shape for the problem of a fluid film being squeezed between two membrane-bound cells figures 5 (*a–c*) would be replotted by halving the film thickness at any time T. The horizontal axis to the replotted graph would then be the plane of symmetry between the two cells. No replotting is necessary for the case of an air bubble pressing against a rigid planar

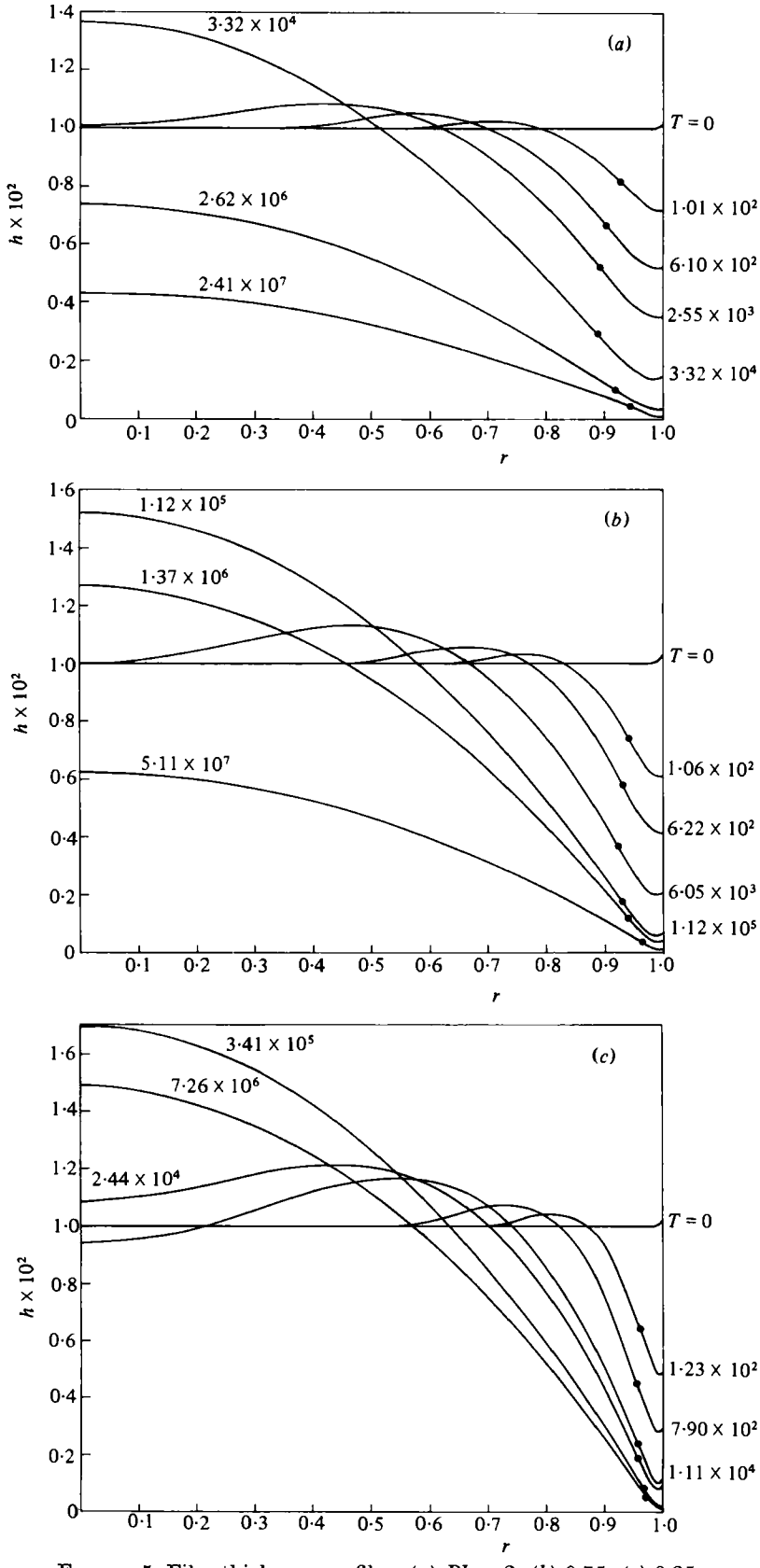

FIGURE 5. Film-thickness profiles: (*a*) $Rl = 2$; (*b*) 0·75; (*c*) 0·25.

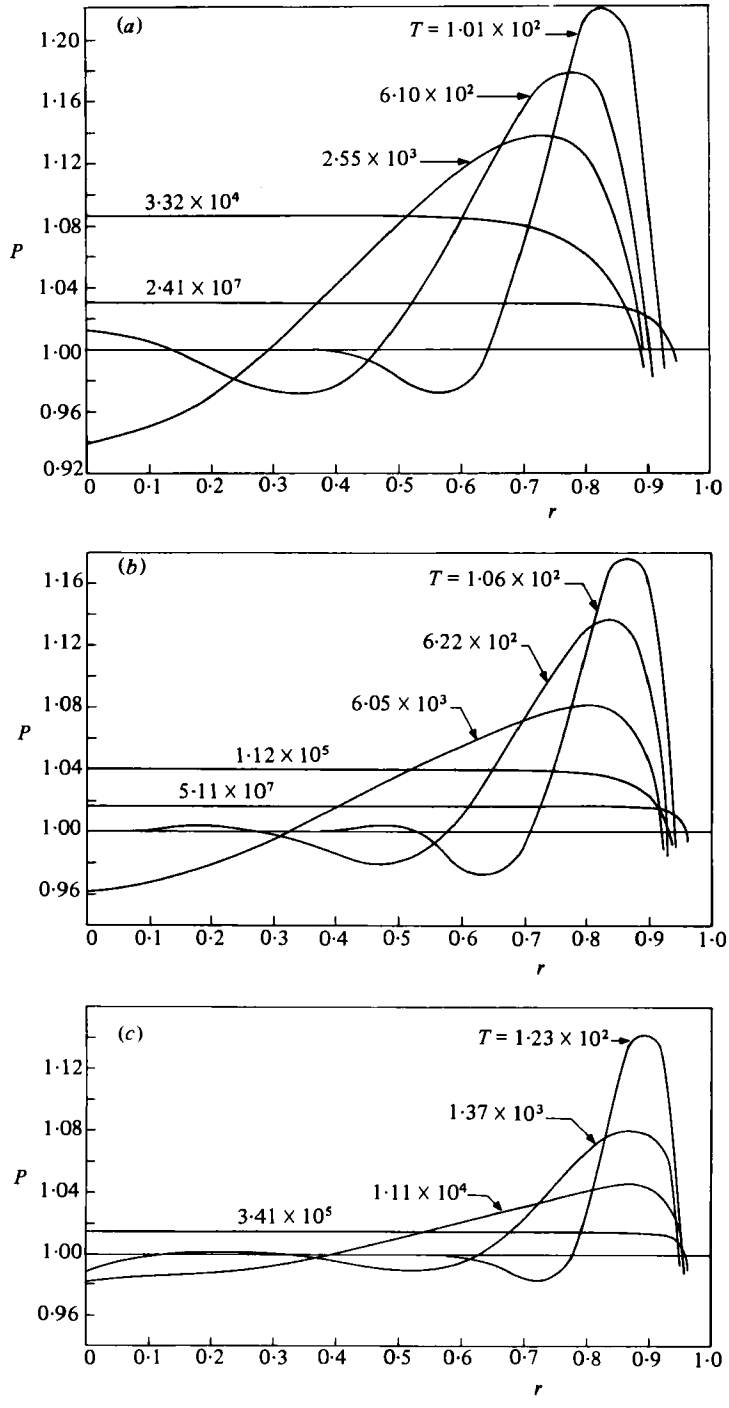

FIGURE 6. Pressure distributions in the fluid film: (*a*) $Rl = 2$; (*b*) 0·75; (*c*) 0·25.

surface. The difference between this problem and the membrane-bound cell enters in the value of β. For the membrane problem $\beta = \pi/6\mu$, whereas for the bubble problem $\beta = 2\pi/3\mu$. From the definition of the non-dimensional time

$$T = \frac{t}{1/\beta(P_c - P_e)}. \tag{3.1}$$

From the values of β for these two situations it is apparent that an air bubble under a solid surface will drain a fluid film four times faster than a membrane-bound cell under identical conditions (i.e. the same values of $P_c - P_e$, Rl, ϵ and μ). Physically, this difference in draining time is connected to the boundary conditions at the cell and bubble surface. The interface between an air bubble and the lubricating film cannot support a fluid shear stress when the viscosity of air is neglected. The shear stress on the surface of a cell membrane tends to retard the fluid motion. The difference between a bubble and a no-slip surface was pointed out in Dimitrov & Ivanov (1978). The difference was manifested in their parameter n, which was equal to 1 for a bubble and 4 for a no-slip surface.

For a cell aspect ratio equal to 2·0 the time histories of the film thickness and pressure distribution in the film are plotted in figures 5(*a*) and 6(*a*) respectively. Because of the order-of-magnitude difference in fluid velocities that are generated during the fluid-trapping and fluid-draining phases of the membrane collapse, the results for volume flow rate are presented in two figures. For a cell aspect ratio equal to 2·0 the volume flow rate for this early period is plotted in figure 7(*a*) and for longer times in figure 7(*b*).

Each time curve in figure 5(*a*) is the instantaneous location of the cell membrane relative to the planar surface. This figure shows the membrane in the vicinity of the edge of the near-contact area collapsing much more rapidly than the membrane in the inner region, thus trapping a considerable volume of fluid in the inner region for dimensionless times less than $3{\cdot}32 \times 10^4$. Figure 6(*a*) shows that the pressure in the fluid film decreases rapidly to the zero exit pressure in the edge region and that a pressure maximum is quickly established just interior to the inner–edge-region matching interface. The difference between the uniform internal pressure P_c and the local film pressure controls the rate of collapse of the membrane. The fluid-trapping phenomenon is a consequence of the large membrane curvatures and pressure differences that can be developed near the edge of this near-contact area and will be examined in more detail below.

One observes in figures 5(*a–c*) that as the edge region descends during the fluid-trapping phase the point of maximum convex curvature lies just interior to the inner-region–edge region interface. For a membrane under one-dimensional loading with uniform tension this point of maximum convex curvature would correspond to the position of maximum film pressure. For axisymmetric loading this correspondence between position of maximum pressure and convex curvature is altered slightly. The location of the pressure maximum also coincides with the location of the flow bifurcation point (see figure 7*a*). The off-axis pressure maximum and the resulting bidirectional flow field during the fluid-trapping phase are not observed in elastohydrodynamic squeeze-film problems. This unique behaviour arises from the membrane tension–curvature relations (2.7) and (2.8). While fluid can be trapped in an elastohydrodynamic squeeze film in the sense that an edge forms as shown in figure 1(*a*) and the maximum displacement of the elastic indenter occurs at the origin, the displacement at the origin decreases monotonically since the approach velocity of the indenter is much greater than its elastic-deformation velocity. The flow is therefore always directed radially outward.

The radial influx of fluid due to the off-axis pressure maximum produces an upward displacement of the membrane between the origin and the flow-bifurcation point. As

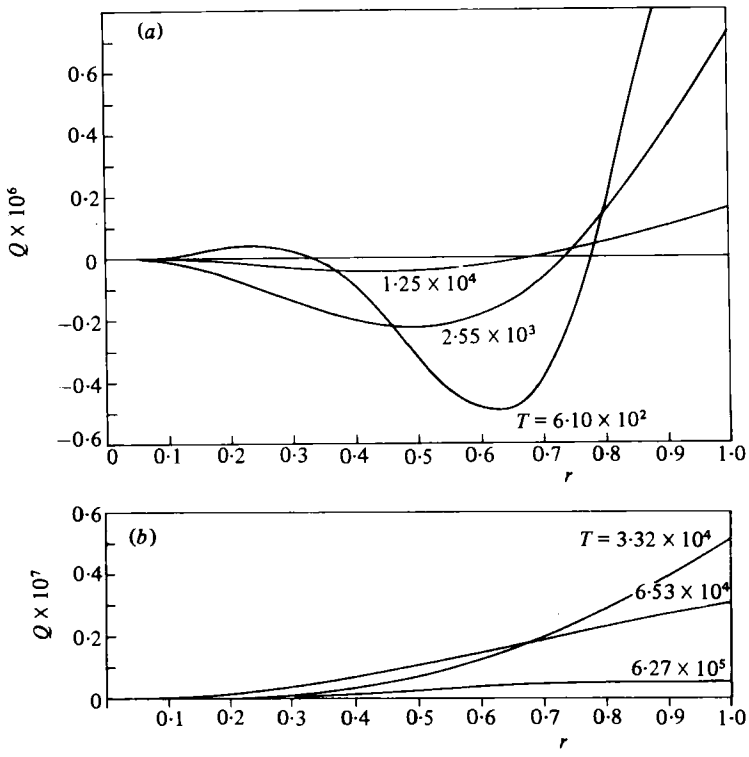

FIGURE 7. Volume flow rate: $Rl = 2$; (*a*) $t < t_{ct}$; (*b*) $t > t_{ct}$.

time increases, the bulge grows in amplitude and migrates to the origin, where the fluid thickness eventually achieves a maximum value at the end of the fluid-trapping phase. During this period of time the pressure peak diminishes in magnitude and migrates slowly toward the origin. The diminished driving force in the lubricating layer results in a decrease in the magnitude of the radial influx of fluid, which vanishes entirely when the pressure maximum reaches the origin (see figure 7*a*).

One also observes in figure 5(*a*) that the location of the inner-region–edge-region interface ($P = 1{\cdot}0$) migrates toward the origin for times smaller than the time for fluid trapping. When the fluid trapping is complete the interface begins an outward migration, which must eventually approach the edge of the near-contact area as T approaches infinity.

For a cell aspect ratio equal to 2·0 the origin film thickness reaches its maximum value at $T = 3{\cdot}32 \times 10^4$. For all later times the off-axis pressure peak is replaced by a characteristic pressure plateau over most of the interior that will be maintained for the duration of the draining process. Also at this time the negative volume flow rate has vanished (figure 7*b*) and the flow field begins to adjust to the downward velocity of the cell membrane near the origin.

From this time on changes in the fluid film occur on a larger time scale. The film-thickness profiles in figure 5(*a*) show that it takes three or more orders of magnitude larger time to drain the trapped fluid than it took to trap it. The pressure plateau has a magnitude of 1·09 at the end of the fluid-trapping phase and three orders of magnitude later in time it still has an appreciable value of 1·03. As time increases the pressure

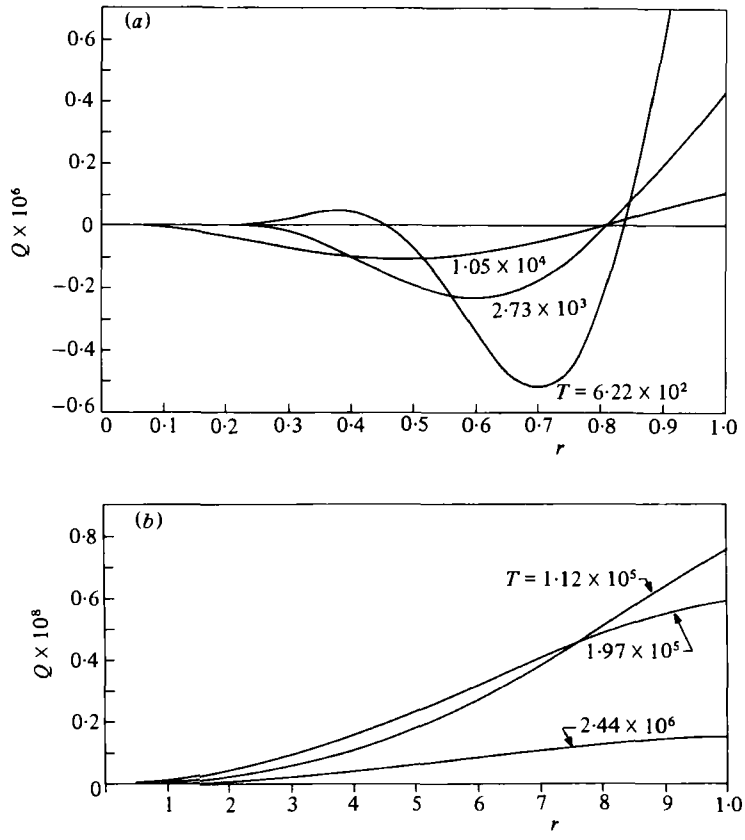

FIGURE 8. Volume flow rate; $Rl = 0{\cdot}75$: (*a*) $t < t_{ct}$; (*b*) $t > t_{ct}$.

plateau both spreads radially and asymptotically approaches the uniform internal cell pressure P_c for the entire near-contact area as T approaches infinity.

The results for h, P and Q for cell aspect ratios 0·75 are presented in figures 5(*b*), 6(*b*) and 8(*a*, *b*) and those for cell aspect ratio 0·25 in figures 5(*c*), 6(*c*) and 9(*a*, *b*). A comparison of these results with the aspect-ratio 2·0 cell just discussed reveals that as the cell aspect ratio is decreased the magnitude of the pressure maximum becomes smaller and shifts closer to the edge of the cell. These changes cause the edge to collapse more quickly for the flatter cell, thus trapping a larger volume of fluid in the inner region. The larger volume of trapped fluid coupled with a smaller fluid driving force results in larger draining times for the flatter cell. This is clearly shown by comparing the film thickness at the origin for cells of aspect ratio 2·0 and 0·25. At the time when the origin film has decreased to 57 % of its initial value for a cell with aspect ratio of 2·0, the flatter cell has drained its origin film to approximately 149 % of its initial value from a maximum of 170 %. Thus, the rate of draining is influenced in large measure by the aspect ratio of the membrane-bound cell as suggested by the order-of-magnitude analysis presented in § 2.

3.1. *Experiments confirming the early-time behaviour*

The bifurcating flow behaviour of the fluid film during the early period following the initial application of the load has not been previously reported. A simple validating

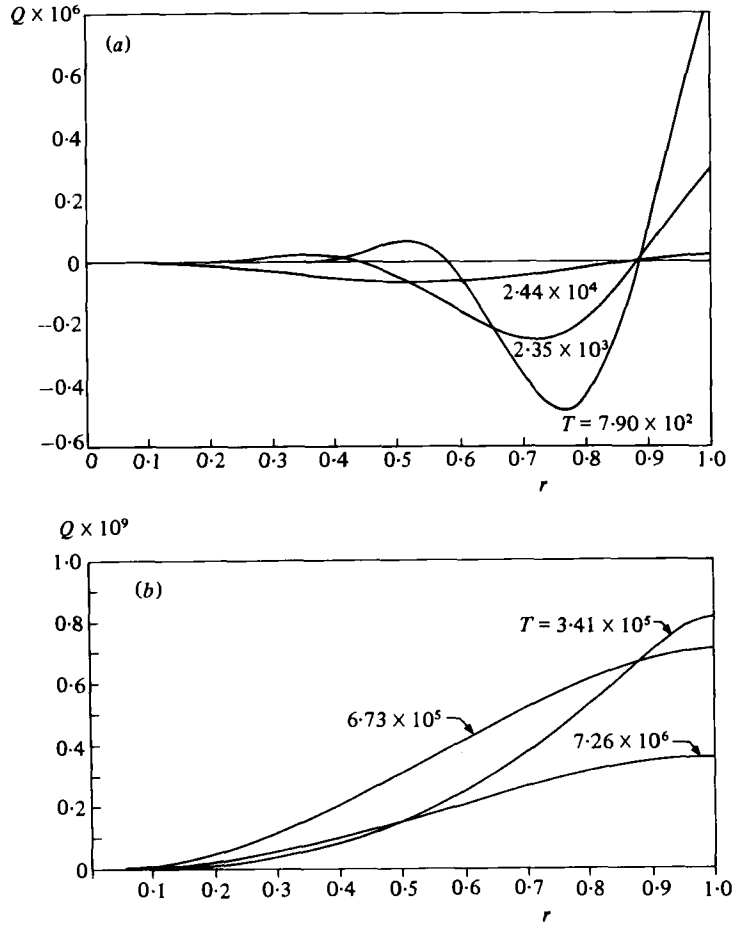

FIGURE 9. Volume flow rate; $Rl = 0{\cdot}25$; (*a*) $t < t_{ct}$; (*b*) $t > t_{ct}$.

experiment was therefore conducted to demonstrate the existence of this unusual fluid-film behaviour.

A schematic representation of the apparatus used to confirm the existence of the bifurcating flow and the fluid-trapping phenomena is depicted in figure 10. An air-filled balloon is used as the model for a membrane-bound fluid cell and a glass plate serves as the rigid planar surface. The fluid film between the plate and balloon is a common vegetable dye. A motor-driven camera is mounted above the glass plate to capture the change in film thickness with time. The camera's motor drive shoots four frames per second, which is sufficiently fast to capture the changes in film thickness because the characteristic time for fluid trapping is of order 5–10 s for this experiment. The radius of the balloon is 7·6 cm and the position of the support blocks produces a near-contact area of 4·1 cm. The non-dimensional aspect ratio is thus equal to 1·84.

The ballloon is coated with the vegetable dye and then the glass plate is dropped onto the supports. The balloon carries 0·9 kg of the plate's mass and the support blocks the remainder of the load. At the instant that the plate makes contact with the support blocks the fluid film is nearly uniform in thickness.

Figure 11 shows the changes in the fluid film during the early period following the

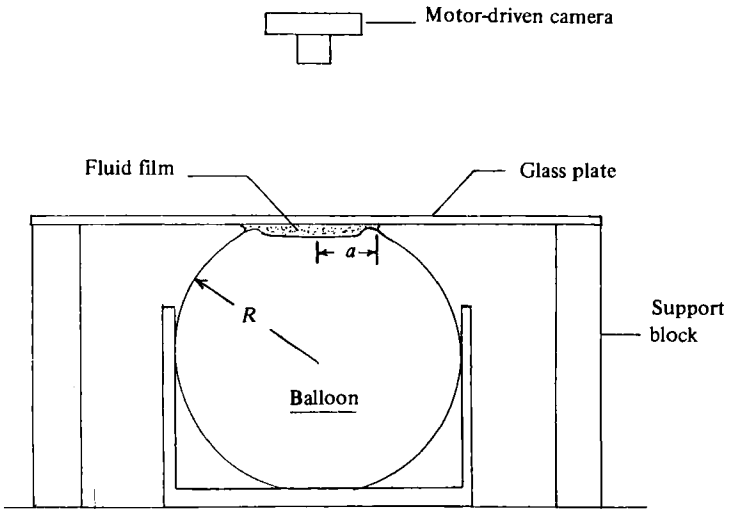

FIGURE 10. Schematic representation of the membrane squeeze-film experiment.

application of the glass plate. Photograph (*a*) in figure 11 is taken at the instant the plate touches the support blocks. Here the contrast of the fluid film is almost uniform, indicating that there is a nearly constant film thickness. In photograph (*b*), after 0·25 s has elapsed, there is a light ring forming at the perimeter of the fluid film. This ring is the edge region and the light region is indicative of a narrowing gap between the plate and the balloon. The dark ring just outside the edge region is a reservoir of dye at the point where the balloon surface falls away from the glass plate. Photographs (*c*) and (*d*) show the growth of the edge region with time.

For this experimental run a small air bubble happened to lie in the edge region. As time passed the air bubble was forced toward the fluid meniscus at the border of the near-contact area, indicating a net decrease in film volume in the near-contact area and a radial outflow from the edge region. Another feature that can be seen in figure 11 is the gradual darkening of the central portion of the near-contact area. This darkening is produced by the gradual thickening of the fluid film near the origin, which is produced by the inward flow of dye predicted by the theory of § 2.2.

The gradual darkening in the central region of the fluid film can be more clearly demonstrated by performing an experiment in which the fluid film near the origin is initially depleted. This is accomplished by lightly pressing the plate against the balloon, producing a small near-contact area. One then allows the fluid to drain in this small area by holding the plate for several seconds. The plate is then released to form the larger near-contact area. Photograph (*a*) in figure 12 shows the light spot surrounding the origin following the release of the plate. Photographs (*b–d*) of figure 12 show the gradual darkening of this area. These photographs clearly show an influx of fluid toward the centre of the lubricating layer.

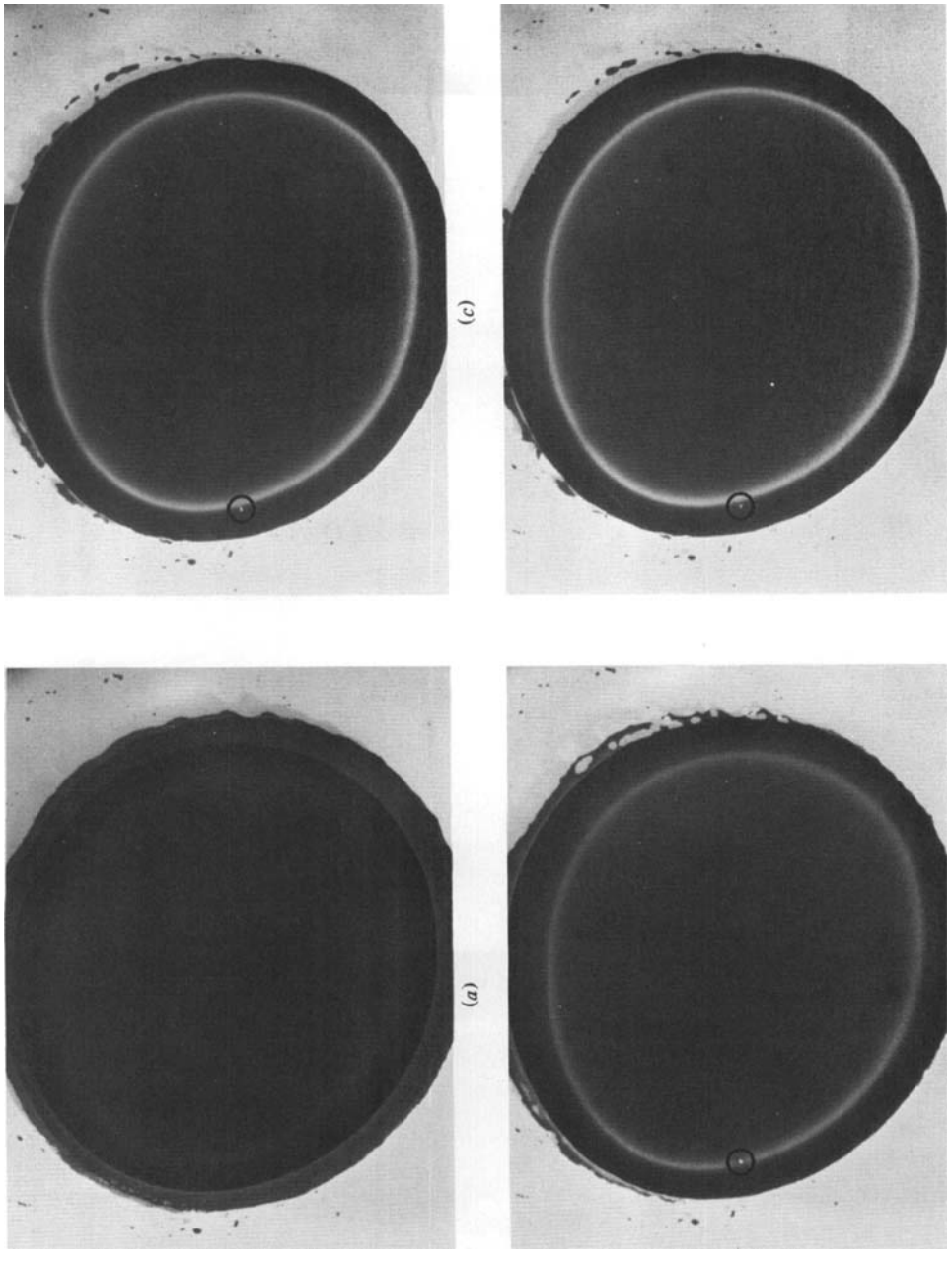

FIGURE 11. Time history of a fluid film being squeezed between a glass plate and an air-filled balloon, showing the formation of the edge region and the dual-flow condition (outward motion of the air bubble and the thickening of the origin fluid film); applied load = 0·9 kg, a = 4·1 cm, Rl = 1·84. (*a*) Time = 0 s; (*b*) 0·25 s; (*c*) 1·25 s; (*d*) 5·50 s.

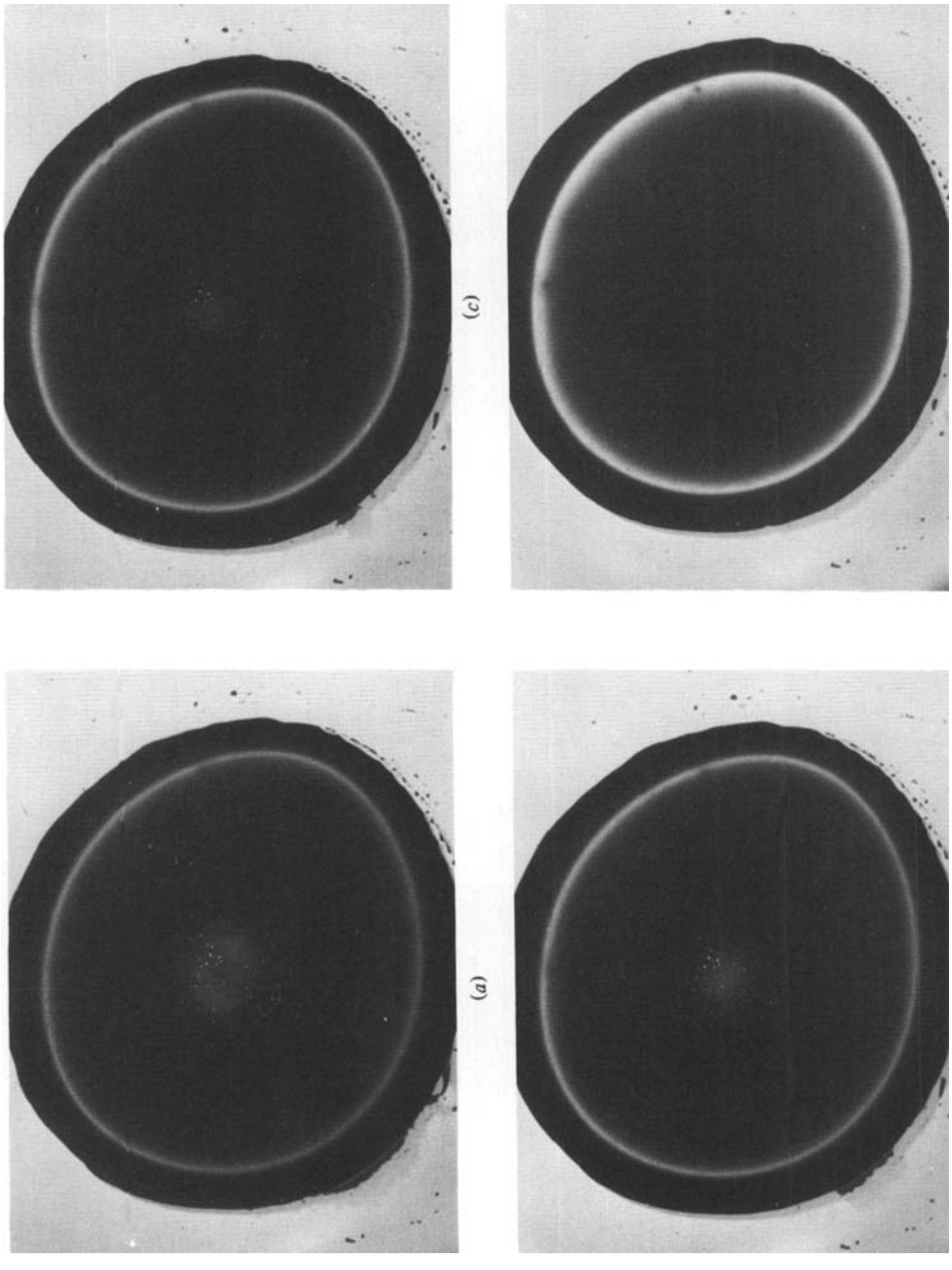

FIGURE 12. Time history of a fluid film, with an initially depleted origin, being squeezed between a glass plate and an air-filled balloon; applied load = 0·9 kg, a = 4·1 cm, Rl = 1·84. (*a*) Time = 0 s; (*b*) 1·0 s; (*c*) 2·0 s; (*d*) 9·0 s.

3.2. *Conclusions*

The membrane squeeze-film theory presented in § 2 predicts the existence of an off-axis pressure maximum and a bidirectional flow in the fluid film for times less than the characteristic time for fluid trapping. This early-time behaviour is easily observed in a simple experiment with a balloon, glass plate and vegetable dye. The experimental photographs clearly illustrate the presence of the bidirectional flow in the dye following the application of the plate. This behaviour appears to be unique to membrane squeeze-film problems. The linear elastic deformation law for elastohydrodynamic squeeze-film problems and the tension–curvature relations for infinitely flexible membrane-bound cells have been shown to produce strikingly different fluid motions. This difference in flow characteristics demonstrates the need for a realistic assessment of the elastic properties of the deformable body before a particular theory is applied. The membrane squeeze-film theory presented in this work is the one most applicable to biological cells with easily deformable phospholipid bilayer membranes.

A logical extension of this work would be to include relative translational motion between the planar surface and membrane-bound fluid-filled cell. This extension of the membrane squeeze-film theory may be applied to the problem of a red blood cell translating through a capillary. The problem of a large air bubble squeezing a fluid film adjacent to a rigid planar boundary inclined at an arbitrary angle, as the bubble slides up along the planar surface due to buoyancy, could also be treated by including translational motion.

The membrane squeeze-film theory has shown the influence that the membrane boundary has on the pressure field developed in the fluid film (off-axis pressure maximum for short times and the pressure plateau for long times). The theoretical treatment of an assemblage of membrane-bound fluid-filled cells at very small porosities undergoing consolidation would have to consider this unusual flow behaviour in the determination of the local excess pore pressure. Laboratory experiments reported in Wu, Pfeffer & Weinbaum (1981) show that large departures from classical consolidation theory occur for void volumes less than 0·15.

This work has been performed in partial fulfilment of the requirements for the Ph.D. degree of R. Wu from the School of Engineering of The City College of the City University of New York. This research has been supported by NSF Grant ENG 78-22101 and NIH Grant RO1 HL19454. The study described herein was completed in the summer of 1980 and presented at the A.S.M.E. Winter Annual Meeting in Chicago, 16–21 November 1980. An earlier version of this paper appeared in *A.S.M.E. Advances in Bioengineering*, 1980.

Addendum

Subsequent to the completion of this paper the authors learned of an equivalent investigation performed by C. Y. Lin and J. C. Slattery at Northwestern University on the thinning of a liquid film as a drop or bubble coalesces at a solid boundary or a fluid–fluid interface (Lin & Slattery 1982). Although the governing equations and boundary conditions for the immobile (highly viscous) drop are the same as (2.20)–(2.23) in the present paper, the behaviour on the short timescale described herein is

fundamentally different from the droplet coalescence problem. This difference arises because of the different initial conditions for the two problems as described in the first footnote at the beginning of § 2. A small drop slowly settling under gravity toward a boundary or interface does not possess a short-time behaviour, since the fluid trapping occurs gradually and on a timescale comparable to the rest of the motion. In the numerical computations of Lin & Slattery the initial conditions are not an undeformed spherical drop, but a somewhat arbitrary initial condition that some time after the motion has started there is a time where the thinning rate of the film at its centre and its rim are equal, and at this instant in time the thinning rate is independent of radial position. For the cell geometry examined in figure 5(*b*) of the present study one observes that this time occurs shortly after $T = 1{\cdot}12 \times 10^5$ or the end of what we have called the fluid-trapping phase. The study of Lin & Slattery thus starts at a time after the motions of principal interest in the present investigation have been completed. This includes the bidirectional fluid motion in the film, the establishment of the off-axis pressure maximum, the thickening of the film at its origin and the initial formation of the edge region. The behaviour for $T > 1{\cdot}12 \times 10^5$ is essentially identical with the computations of Lin & Slattery.

Another point that needs to be emphasized is the relative magnitudes of the different time and space scales involved. The motion of interest in the present investigation occurs on a timescale two or more orders of magnitude shorter than the behaviour of interest in drop-coalescence studies. Similarly, the latter problem does not have narrow spatial regions with steep gradients. While a narrow gap does form in small-drop coalescence, the radial width of the gap is not small compared with the lengthscale of the inner region. A single uniformly valid numerical solution procedure could therefore be employed. In contrast, a more-elaborate two-region inner and outer numerical solution technique had to be employed in the present study since the edge region was confined to a small fraction of the near-contact area. In fact, the authors at the beginning of the present study attempted to use a single region numerical calculation equivalent to that of Lin & Slattery but could not get the numerical finite-difference scheme to work.

REFERENCES

BARNARD, A., LOPEZ, L. & HELLUMS, J. D. 1968 *Microvas. Res.* **1**, 23.

BENJAMIN, M. K. 1969 Compliant surface bearings: an analytic investigation. Doctoral thesis, Columbia University, New York.

BRETHERTON, F. P. 1961 *J. Fluid Mech.* **10**, 166.

BROWNE, A. L., WHICKER, D. & ROHDE, S. M. 1975 *Tire Sci. Tech.* **3**, 16.

CASTELLI, V., RIGHTMIRE, G. K. & FULLER, D. D. 1967 *Trans. A.S.M.E.* F, *J. Lubric. Tech.* **89**, 510.

CHRISTENSEN, H. 1962 *Proc. R. Soc. Lond.* A **266**, 312.

CHRISTENSEN, H. 1970 *Trans. A.S.M.E.* F, *J. Lubric. Tech.* **92**, 145.

COX, B. G. 1962 *J. Fluid Mech.* **14**, 81.

DAVIS, R. M. & TAYLOR, G. I. 1949 *Proc. R. Soc. Lond.* A **200**, 375.

DIMITROV, D. S. & IVANOV, I. B. 1978 *J. Colloid Interface Sci.* **64**, 97.

DOWSON, D. & HIGGINSON, G. R. 1960 *J. Mech. Engng Sci.* **2**, 188.

FITZ-GERALD, J. M. 1969 *Proc. R. Soc. Lond.* B **174**, 193.

GAMAN, I. D. C., HIGGINSON, G. T. & NORMAN, R. 1974 *Wear* **28**, 345.

GOLDSMITH, H. L. & MASON, S. G. 1962 *J. Fluid Mech.* **14**, 42.

HARTLAND, S. 1967 *Trans. Instn Chem. Engrs* **45**, 97.

HARTLAND, S. 1968 *J. Colloid Sci.* **26**, 283.

HARTLAND, S. 1969 *Chem. Engng Sci.* **24**, 987.

HERREBRUGH, K. 1970 *Trans. A.S.M.E.* F, *J. Lubric. Tech.* **92**, 292.

HILDEBRAND, F. B. 1976 *Advanced Calculus for Applications.* Prentice-Hall.

HOCHMUTH, R. M., MARPLE, R. N. & SUTERA, S. P. 1970 *Microvas. Res.* **2**, 409.

HYMAN, W. A. & SKALAK, R. 1970 Viscous flow of a suspension of deformable liquid drops in a cylindrical tube. *Tech. Rep.* no. 5, *Project* NR 062-393, *Dept of Civil Engng and Engng Mech., Columbia University.*

JONES, A. F. & WILSON, S. D. R. 1978 *J. Fluid Mech.* **87**, 263.

LEE, J. S. & FUNG, Y. C. 1969 *Microvas. Res.* **1**, 221.

LEE, K. M. & CHENG, H. S. 1973 *Trans. A.S.M.E.* F, *J. Lubric. Tech.* **95**, 308.

LIGHTHILL, M. J. 1968 *J. Fluid Mech.* **34**, 113.

LIN, K. L., LOPEZ, L. & HELLUMS, J. D. 1973 *Microvas. Res.* **5**, 7.

LIN, C. Y. & SLATTERY, J. C. 1982 *U.S. Dept. of Energy: Fossil Energy Rep.* DOE/BC/10068-16. To be published.

PRINCEN, H. M. 1963 *J. Colloid Sci.* **18**, 178.

PROTHERO, J. W. & BURTON, A. C. 1961 *Biophys. J.* **1**, 565.

PROTHERO, J. W. & BURTON, A. C. 1962 *Biophys. J.* **2**, 199.

ROBERTS, A. D. 1974 Lubrication studies of smooth rubber contacts. In *The Physics of Tire Traction, Theory and Experiment* (ed. D. F. Hays & A. L. Browne). Plenum.

ROHDE, S. M., WHICKER, D. & BROWNE, A. L. 1976 *Trans. A.S.M.E.* F, *J. Lubric. Tech.* **98**, 401.

SCHRYER, N. L. 1977 Numerical solution of time-varying partial differential equations in one space variable. *Bell Lab. Comp. Sci. Tech. Rep.* no. 53.

SESHADRI, V., HOCHMUTH, R. M., CROCE, P. A. & SUTERA, S. P. 1970 *Microvas. Res.* **2**, 434.

SKALAK, R. 1972 Mechanics of the microcirculation. In *Biomechanics: Its Foundation and Objectives* (ed. Y. C. Fung, N. Perrone & M. Anliker), p. 457. Prentice-Hall.

SUTERA, S. P., SESHADRI, V., CROCE, P. A. & HOCHMUTH, R. M. 1970 *Microvas. Res.* **2**, 420.

TÖZEREN, H. & SKALAK, R. 1978 *J. Fluid Mech.* **87**, 1.

TÖZEREN, H. & SKALAK, R. 1979 *J. Fluid Mech.* **95**, 743.

WHICKER, D., BROWNE, A. L. & ROHDE, S. M. 1976 *J. Fluid Mech.* **78**, 247.

WU, R. 1981 Ph.D. dissertation. City University of New York.

WU, R., PFEFFER, R. & WEINBAUM, S. 1981 Consolidation of a cellular fluid matrix; a simplified model of the cellular component of the artery wall. Submitted for publication.